3. PHOTOELASTIC STUDY OF TWO BIAXIAL STRESS FRACTURE SPECIMENS

by

C.R. Wachnicki and J.C. Radon

Department of Mechanical Engineering
Imperial College of Science and Technology
London SW7 2BX, England

ABSTRACT

The present paper considers the applicability of two fracture specimens, one a model in actual use (specimen A), and the other one specially designed for the purpose (specimen B), for the investigation of crack growth under tensile biaxial stress. A photoelastic stress analysis of the two fracture specimens in their testing environment leads to the establishment of reasonably uniform stress biaxiality and symmetry in the working region. The separation of the principal stresses is calculated from the two quantities of stress difference and stress sum. The former is obtained from isochromatics and the latter from isopachics evaluated by means of a numerical method based on Laplace's equation.

Design, construction and mode of operation of the testing equipment are described and the results of the experiments conducted on suitable photoelastic material - Araldite CT200 - are then evaluated. These results indicate that the uniform working region of the new specimen is relatively larger and more suitable for biaxial loading than that of the original design.

NOMENCLATURE

A_t	:	transverse area of cross section
B	:	load biaxiality ratio
B_l	:	local biaxiality ratio
B_n	:	nominal biaxiality ratio
dx, dy	:	lattice spacings
F	:	model fringe value
G, g_1, g_2, g_3, g_4	:	dimensionless constants
n	:	fringe order
P_y, P_x	:	nominal load, transverse load
s, b	:	parameters for fractional lattice spacings
σ_1, σ_2	:	principal normal stresses
σ_y, σ_x	:	normal stresses on planes perpendicular to the y and x axis
σ_{nom}	:	nominal stress as defined by P_y/A_t
Φ	:	stress sum = $\sigma_1 + \sigma_2$

INTRODUCTION

In investigating certain phenomena such as fatigue crack growth in large plates under biaxial stress, it is desirable to produce a well defined two-dimensional stress field in a specimen. In this field, it is not only requisite that the two principal stresses be of known magnitude, but also that they should be exactly constant over a considerable area. The application of existing concepts and techniques of fracture mechanics used in analysing crack growth behaviour has generally been confined to uniaxial stress situations, while biaxial stress situations have been less widely investigated. However, recent research in our department (1,2) provides a comprehensive survey of work already done on fatigue crack growth in polymethylmethacrylate (PMMA) under biaxial stress and reports on various aspects of crack growth such as fracture toughness (3,4,5,6), fatigue crack growth rates (4,7,8), instability of crack path direction (9), and slow crack growth rates in viscoelastic materials (10), are now available. The most common of the fracture problems is fatigue, in which cracks may be expected to initiate and propagate continuously along a minor principal stress trajectory (11,12). The situation is further complicated as the ratio between the two principal stresses may vary considerably during propagation. Workers in close contact with experimental stress analysis are aware of the complications besetting this problem and of the need for further investigation into biaxial stress fracture testing. But before this can be initiated, the development of a suitable specimen geometry for biaxial stress testing is required.

The photoelastic study of biaxial stress fracture specimens described in this paper offers the invaluable advantage of providing an overall picture of their stress distribution. For the determination of individual stresses in a biaxial stress field, however, isochromatic information does not suffice, and the need for supplementary information is satisfied by auxiliary techniques applied to complement the photoelastic method, i.e. the isopachic method.

The value of photoelasticity in solving engineering stress problems in two dimensions has been amply demonstrated by a number of investigations, notably those carried out by Coker & Filon (13,14). Other technical applications have been discussed by Frocht (15), Durelli & Riley (16), and the work of Jessop & Harris (17) contains a wide range of important examples.

In order to obtain a photographic record of a large area of the model as well as the projection of a bright image on to a large screen to map isochromatic

fringe orders, a transmission polariscope of the lens type was selected. The characteristics of polariscopes are described by Mylonas (18) and Mindlin (19), while Mehrotra (20) discussed the effects and remedies of non-uniform illumination in lens polariscopes, and will not be elaborated further here.

The machine used for biaxial stress fatigue testing in the present work (Figure 1) is one described in (2). A single hydraulic actuator applies in-phase tensile loads to both axes by means of a simple mechanical linkage. In general, the load point of the actuator can be varied to change the load biaxiality ratio, B, defined as the normal load P_y divided by the transverse load P_x. The present arrangement allows biaxiality ratios, B_n, of 0, 1, 1.5, 2, 3 and 4. Easy visual access to the specimen, indispensible in crack monitoring and transmission photoelastic work, is provided by the straining frame, to which a specially built lens polariscope can be attached.

TWO BIAXIAL STRESS FRACTURE SPECIMENS

The realisation that fracture studies require a specimen in which a crack can propagate over a reasonably large distance in a controlled stress field not drastically modified by its presence has led researchers to adopt cruciform and square plate specimens.

In their investigation of fatigue crack propagation in biaxial stress fields, Hopper & Miller (21) used a cruciform specimen whose design was similar to that described by Mönch & Galster (22), except for the central section which had been reduced in thickness by a factor of four. Within a working region of 76 mm square, compatible with the available machine space and load capacity, this design produced an approximately 45 mm square area of uniformly strained plate.

Subsequently, Mönch & Galster (22) described the difficulties involved in modifying the square plate configuration for biaxial loading, while Cridland & Wood (23) compared square plate and cruciform geometries and showed that the latter had reduced stress concentrations and that the extent of the isotropic region increased as far as to cover virtually the whole of the central square when subjected to equibiaxial stress.

Johnson & Khan (24) used a specimen similar to that described in (22) for creep fracture studies, loading it through a "whipple tree" linkage, a loading device which permits some misalignment of the loading pin holes and non-uniform relaxation of the specimen during the test while maintaining constant stress rather than constant displacement boundary conditions. It was the very principle of whipple tree linkage that motivated the present design of a set of load distributing shackles for the current fracture specimen. It was also the reliance on the sources referred to above (22,23,24) which influenced the original design of the biaxial stress specimen shown in Figure 2. The load distributing shackles are illustrated as an assembly in Figure 3.

The new improved design evolved in the present work (Figure 4) was based, to a certain extent, on the work of Mönch & Galster. The load was applied to the central region which was assumed, for the purpose of analysis, to be a square plate of 100 mm width under uniform normal boundary stresses through nine narrow shanks on each side of the specimen. The longer and more compliant these shanks were, the less the influence of the transverse strain affected the applied stress normality. A model was machined from a cast sheet of Araldite CT200 (ICI), 6 mm thick. When force was applied to the ends of the model, the vertical displacements of all points of the clamped end became, under loading conditions,

equal all over the breadth of the clamping region. Clamping was carried out over an area of 100 by 30 mm; uniformity in the clamping region was obtained by inserting double layers of emery cloth between the model and clamping jaws. To ensure this uniformity of breadth, the authors had to resort to the use of specially designed rigid steel clamps. To avoid initial stresses when loading, the clamping pressure had to be as uniform as possible.

A PROCEDURE FOR THE NUMERICAL SOLUTION OF LAPLACE'S EQUATION

The isopachic method is very attractive when used in conjunction with the normal room temperature photoelastic technique as it produces a fine network of the two principal stresses over the entire region under investigation.

Numerical methods have proved most practical in the solution of Laplace's equation and the determination of isopachic patterns, first introduced by Weller & Shortley (25). The relaxation method developed by Southwell (26) is very suitable for treating difference equations such as the improvement formula.

It can be shown in any treatise on the theory of elasticity (27) that the sum of the principal stresses ($(\sigma_1 + \sigma_2)$ or Φ) in a model in which the conditions for generalised plane stress are satisfied in a solution of Laplace's equation is:

$$\frac{\partial^2 \Phi}{\partial x^2} + \frac{\partial^2 \Phi}{\partial y^2} = 0 \qquad (1)$$

The stress sum values along the model boundary were required to solve this equation for a given region. These were conveniently obtained from the isochromatic fringe photograph of the model. For purposes of calculation, it was desirable to use an artificial boundary which avoids loaded parts of the actual boundary. In the case of specimen A, the stress values on the artificial boundary were supplemented with lateral extensometer stress sum values. The procedure for specimen B was different in that the boundary values were obtained by considering the stress distribution in the regions of the fillets and the shanks. It was assumed the narrow shanks carried pure tensile loads and so the actual boundary values were obtained solely from isochromatic data.

The procedure followed in this numerical determination requires the establishment of a square network on a scale drawing of the model. The improvement formula (equation (2)) requires that the value Φ at any point in such a square net to be the mean of its four nearest equidistant neighbours:

$$\Phi_o = (\Phi_1 + \Phi_2 + \Phi_3 + \Phi_4)/4 \qquad (2)$$

An improved equation (equation (3)) is formulated by (25) for complex stress distributions, i.e. in the boundary region, and is illustrated in Figure 5:

$$\Phi_o = (4(\Phi_1 + \Phi_2 + \Phi_3 + \Phi_4) + \Phi_5 + \Phi_6 + \Phi_7 + \Phi_8)/20 \qquad (3)$$

If the spacings are not equal, i.e. near the curvature of the fillet boundary, a similar but more complex expression can be derived which takes the form:

$$\Phi_o = G(g_1 \Phi_1 + g_2 \Phi_2 + g_3 \Phi_3 + g_4 \Phi_4) \qquad (4)$$

In this equation, the values of the constants depend upon the distances of the neighbouring points of interest. For the case shown in Figure 6, the constants have the following values: $G = sb/(s+b)$; $g_1 = 1/(1+s)$; $g_2 = 1/(1+b)$; $g_3 = 1/(s(1+s))$; $g_4 = 1/(b(1+b))$.

As there are as many sets of improvement equations as there are interior points of the net, Liebmann (28) has suggested a convenient iterative procedure for solving these equations for the unknown values of Φ at the interior points. The procedure was initiated by assigning appropriate values to a number of interior points of a net calculated from the actual loads on the particular specimen. The square network was laid down on a quarter section of the two models, which are symmetrical about two perpendicular axes, the position of the net being such that a line of points lies along both axes of symmetry. These points are improved in the usual way by assuming that values on opposite sides of the line are equal and are improved simultaneously.

It is advisable to start by solving the difference equations with a very coarse net and then successively cut the net spacing in half. The previous solutions of the coarser nets are desirable because each halving of the net constant, the convergence is about four times as slow. The reduction of the net spacing is stopped when the desired accuracy in the solution has been achieved, which may not be greater than the accuracy with which the boundary values are known. In the tests, a square lattice was laid over the region in question with lattice spacings ranging from 0.5 to 4 mm in an area 50 by 50 mm for specimen B and 95 by 95 mm for specimen A.

The values calculated from this iteration were transferred to a finer net. One part of the coarse net was covered by the fine net in close proximity to the boundary leaving out the central square of the model which remained covered

by the coarse net as shown in Figure 7. The extent of the fine mesh in the working region depends on the size of the uniformity in the central region of the specimen shown by the isochromatic patterns. This density of the net is desirable near the region of the boundary where the function of Φ curves very rapidly and is also economical of computer time. For the net work suggested in Figure 7, the appropriate formulae are:

$$\Phi_c = (\Phi_a + \Phi_b + \Phi_d + \Phi_g)/4 \quad ; \quad \Phi_k = (\Phi_g + \Phi_l + \Phi_j + \Phi_m)/4 \qquad (5)$$

$$\Phi_g = (2\Phi_c + 3\Phi_f + \Phi_k + 3\Phi_h)/9 \quad ; \quad \Phi_f = (4\Phi_b + 5\Phi_e + \Phi_j + \Phi_k + 5\Phi_g)/16$$

Once the nets have been drawn, the boundary values were read into the program with selected values for the interior points. The value at each interior point was then improved by traversing the network in a definite sequence while using the above discussed equations. Each time the network was traversed, the values were further improved. The iteration process was continued until the stress sum values at each point reproduce themselves or satisfy the convergence criterion.

EXPERIMENTAL PROCEDURES AND RESULTS

Four experiments in all were carried out on both specimens for nominal biaxiality ratios of B_n = 0 and 2. Maps of isochromatics were obtained using a specially constructed lens polariscope, the parts of the lens polariscope were mounted on a frame which was rigidly bolted to the welded frame of the fatigue testing machine as shown in Figures 8 and 9. Arrangement of polariscope elements for isochromatics and a method for counting isochromatic fringes can be found in most text books on photoelasticity (16). For specimen A, the isopachic maps were obtained using a combination of photoelastic and lateral extensometer data along an artificial boundary. A similar procedure was followed with specimen B, except that the isopachic maps were determined by using boundary conditions obtained solely from photoelastic data.

In test 1, specimen A was loaded uniaxially (B_n = 0) through the numerous pin-jointed linkages of the specimen until a fourth order fringe manifested itself at the centre of the specimen in the viewing screen for a normal load of P_y = 7.85 kN. From the following equation, stress difference:

$$(\sigma_y - \sigma_x) = n F \qquad (6)$$

and for this test, n = 4 and F = 1.64 MN/m^2.fr, therefore $\sigma_y - \sigma_x$ = 6.56 MN/m^2 at the centre. The model fringe value, F, was obtained from a small tensile model machined from the same material as the specimen. The map of isochromatics for this test is shown in Figure 10, and Figure 11 shows the isopachic map obtained by applying the numerical technique. The individual stresses were calculated from the above figures by means of two equations:

$$\sigma_y = \{(\sigma_y + \sigma_x) + (\sigma_y - \sigma_x)\}/2 \qquad (7)$$

$$\sigma_x = \{(\sigma_y + \sigma_x) - (\sigma_y - \sigma_x)\}/2 \qquad (8)$$

the results of which are shown as a variation of σ_y as a percentage of σ_y at the centre (Figure 12).

In test 2, specimen A was pin loaded biaxially (B_n = 2) until a second

fringe order was observed at its centre. The local biaxiality ratio, B, measured from the X/Y plotter, was 2.05 for a normal load P_y = 7.6 kN and transverse load P_x = 3.7 kN, i.e. $B = P_y/P_x$. The stress difference at the centre was found to be $\sigma_y - \sigma_x$ = 3.28 MN/m^2. Figures 13 and 14 show the isochromatic pattern and the isopachic map, while Figure 15 shows a map of local biaxiality ratio.

In test 3, specimen B was loaded uniaxially through heavy steel clamps until a relatively high fringe order of eight was observed for the normal load of P_y = 8.43 kN. The stress difference at the centre was calculated; $\sigma_y - \sigma_x$ = 13.12 MN/m^2. The maps of isochromatics and isopachics are shown in Figures 16 and 17, respectively. The results of the two patterns are illustrated in Figure 18, the same as for specimen A, $B_n = 0$.

In the final test, specimen B was loaded biaxially ($B_n = 2$) until it reached the third fringe order corresponding to a stress difference of $\sigma_y - \sigma_x$ = 4.92 MN/m^2 at the centre. The normal load was P_y = 5.95 kN and transverse load was P_x = 2.9 kN leading to a load biaxiality ratio of B = 2.05. The results of this test are shown in Figures 19 to 21.

For reasons of comparison and simplicity, no actual stresses were computed, all data being given in equivalent fringe order.

DISCUSSION AND CONCLUSION

During the normal room temperature photoelastic tests for specimen B, the central square of the model appears completely dark for nominal biaxiality ratios of 0 and 2. These tests have proved eminently suitable for the examination of the uniformity of the tension fields and of the very efficiency of the method itself. Comparisons with specimen A for the corresponding biaxiality ratios show the improvement in the homogeneity of the isochromatic field.

The work reported here has brought to light that photoelastic stress separation methods alone do not yield satisfactory results if a high degree of accuracy is required. The isopachic method was chosen to determine the two principal stresses in a plane field not only because of its accuracy but also because of its ability to give an overall picture of the stress distribution. In a particular loading mode, $B_n = 0$, it had to be proved that the second principal stress, σ_2, was negligible when compared with σ_1. If it was to be used as a criterion, the stress σ_2 of the order of 1% of σ_1 had to be measured accurately. This accuracy was achieved in specimen B when it was subjected to a high fringe order of eight with a measuring accuracy of 0.05 fringe, using the Tardy Compensation Method and the Isopachic Method.

A resumé of the results is given in Table I. As the data in the table demonstrate, the new specimen is evidently not only adequate for its intended purpose but also more efficient than the design A.

The results of the experiments show that design B is able to create a practically uniform unidirectional stress field in the central square of the specimen. By the nature of the way the loads are applied to the specimen, it follows that any desired two-dimensional tension state can be produced by biaxial loading, as perpendicular homogeneous pure tension, P_x, can be superposed on the specimen which is independent of P_y.

Close observation of the isochromatic fringes revealed that the fringe pattern was more complex and extensive in specimen A than in specimen B. This was entirely due to the loading conditions, fringe order and the geometry of the model. The influence of the disturbing lateral effect was only slight in specimen B, but was more evident in specimen A. Even so, the central shanks of specimen B showed a much higher fringe order than the edge strips of the uniaxial case, probably because of the absence of constraint on the model in the transverse direction which suggests that the specimen is more efficient in the

biaxial mode for which it is designed.

The isopachic method has the tendency to smooth out the stress distribution in regions where the function Φ is complex, i.e. the boundary region. This characteristic of the method makes it completely dependent on the nature and magnitude of the boundary values insofar as the stress at the centre of the specimen is concerned. Moreover, as the stresses are evaluated from the boundary to the centre of the specimen, one cannot but suspect a tendency to a decrease in the accuracy of the values obtained at the centre. The efficiency of the method will, therefore, depend on the size of the region under investigation and the right choice of net spacing and improvement formula, while its accuracy will be mainly affected by the convergence criterion and the accuracy of the boundary values.

In conclusion, the normal room temperature photoelastic technique, together with the isopachic method, has proved that, for nominal biaxiality ratios of B_n = 0 and 2, a larger uniform state can be achieved in specimen B than in specimen A. For a particular case of B_n = 2, analysis has shown that the local biaxiality ratio varies less than 3% within a central square representing an area 52% of the effective working region for specimen B, but only 29% for specimen A. It follows that specimen B is ideally suited for use in a two-dimensional stress state in which both the principal stresses are tensile but of arbitrary magnitude.

REFERENCES

1. Leevers, P.S. "Fatigue Crack Growth Under Biaxial Stress", M.Sc. Thesis, London University (1975).
2. Leevers, P.S., Radon, J.C. & Culver, L.E. "Crack Growth in Plastic Panels Under Biaxial Stress", Polymer, 17, (7), 627-632 (1976).
3. Hilton, P.D. "Plastic Intensity Factors for Cracked Plates Subjected to Biaxial Loading", Int. J. Fract., 9, 149 (1973).
4. Kibler, J.J. & Roberts, R. "The Effect of Biaxial Stresses on Fatigue and Fracture", J. Eng. Ind., 92, 727 (1970).
5. Smith, S.H. "Analysis of Energy Quantities for Fracture Under Biaxial Stress", Conf. Prospects Fract. Mech., Delft, Netherlands (1974).
6. Sih, G.C. & Liebowitz, H. "On the Griffith Criterion for Brittle Fracture", Int. J. Solids Struct., 3, 1 (1967).
7. Joshi, S.R. & Shewchuck, J. "Fatigue Crack Propagation in a Biaxial Stress Field", J. Exp. Mechs., 10, 529 (1970).
8. Adams, N.J.I. "Some Comments on the Effect of Biaxial Stress on Fatigue Crack Growth and Fracture", Eng. Fract. Mech., 5, 983 (1973).
9. Cotterell, B. "Notes on the Path and Stability of Cracks", Int. J. Fract. Mech., 2, 526 (1966).
10. Laheru, K.L., Hufferd, W.L. & Jacobs, H.R. To be published, Int. J. Fract.
11. Arad, S. Ph.D. Thesis, London University (1972).
12. Klein, G. "Stress Intensity Factors in the Neighbourhood of a Circular Hole and Their Influence on Crack Behaviour", J. Mater. Technol., 6, 30 (1975).
13. Coker, E.G. & Filon, L.N.G. "A Treatise on Photoelasticity", Cambridge University Press (1931); re-issued with Introduction by H.T. Jessop (1957).
14. Filon, L.N.G. "A Manual of Photoelasticity for Engineers", Cambridge University Press (1936).
15. Frocht, M.M. "Photoelasticity", Wiley & Sons, New York, I (1941), II (1948).
16. Durelli, A.J. & Riley, W.F. "Introduction to Photomechanics", Prentice-Hall Incorporated, New Jersey (1965).
17. Jessop, H.T. & Harris, F.C. "Photoelasticity", Cleaver-Hume Press, London (1949); reprinted by Dover Publications (1960).
18. Mylonas, C. "The Optical System of Polariscopes", J. Sci. Inst., 25, 77-87 (1948).

19. Mindlin, R.D. "A Review of the Photoelastic Method of Stress Analysis", J. Appl. Phys., 4, 222-241 (1933); and 10, 273 (1939).

20. Mehrotra, C.L. "On Non-Uniform Illumination in a Lens Polariscope and Remedies", J. Strain Anal., 12, (3), 180 (1977).

21. Hopper, C.D. & Miller, K.J. "Fatigue Crack Propagation in Biaxial Stress Fields", J. Strain Anal., 12, 23 (1977).

22. Mönch, E. & Galster, D. "A Method for Producing a Defined Uniform Biaxial Stress Field", B.J.A.Ph., 14, 810-812 (1963).

23. Cridland, L. & Wood, W.G. "A Hydrostatic Tension Test of a Brittle Material", Int. J. Mech., 4, (3), 277 (1968).

24. Johnson, A.E. & Khan, B. "A Biaxial Stressing Creep Machine and Extensometer" in "Machines for Materials and Environmental Testing", I.Mech.E./S.E.E. (1966).

25. Weller, R. & Shortley, G.H. "The Numerical Solution of Laplace's Equation", J. Appl. Phys., 9, (5), 334 (1938).

26. Southwell, R.V. "Relaxation Methods in Theoretical Physics", Oxford University Press, New Jersey (1946).

27. Timoshenko, S. "Theory of Elasticity", McGraw-Hill Book Company, New York (1934).

28. Liebmann, H. "Die Angenaherte Ermittlelung Harmonischer Funktionen und Konformer Abbildungen", Sitzungberichte der Bayerischen Akademie der Wissenschaften zu München, Mathematische Physikalische Klasse, 382 (1918).

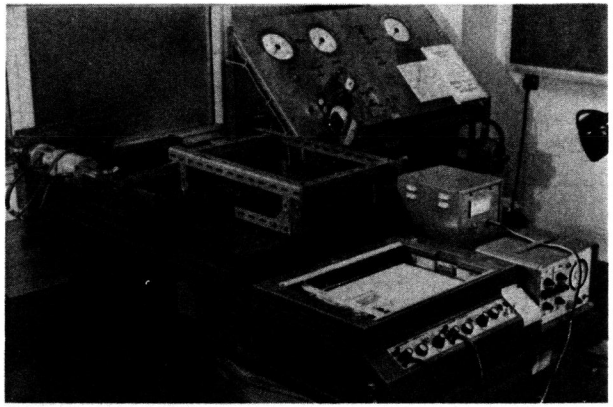

Figure 1: Biaxial Fatigue Machine.

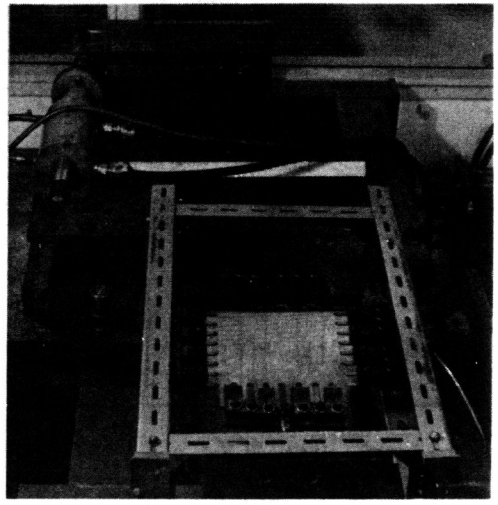

Figure 3: Actuator and specimen shackle assembly.

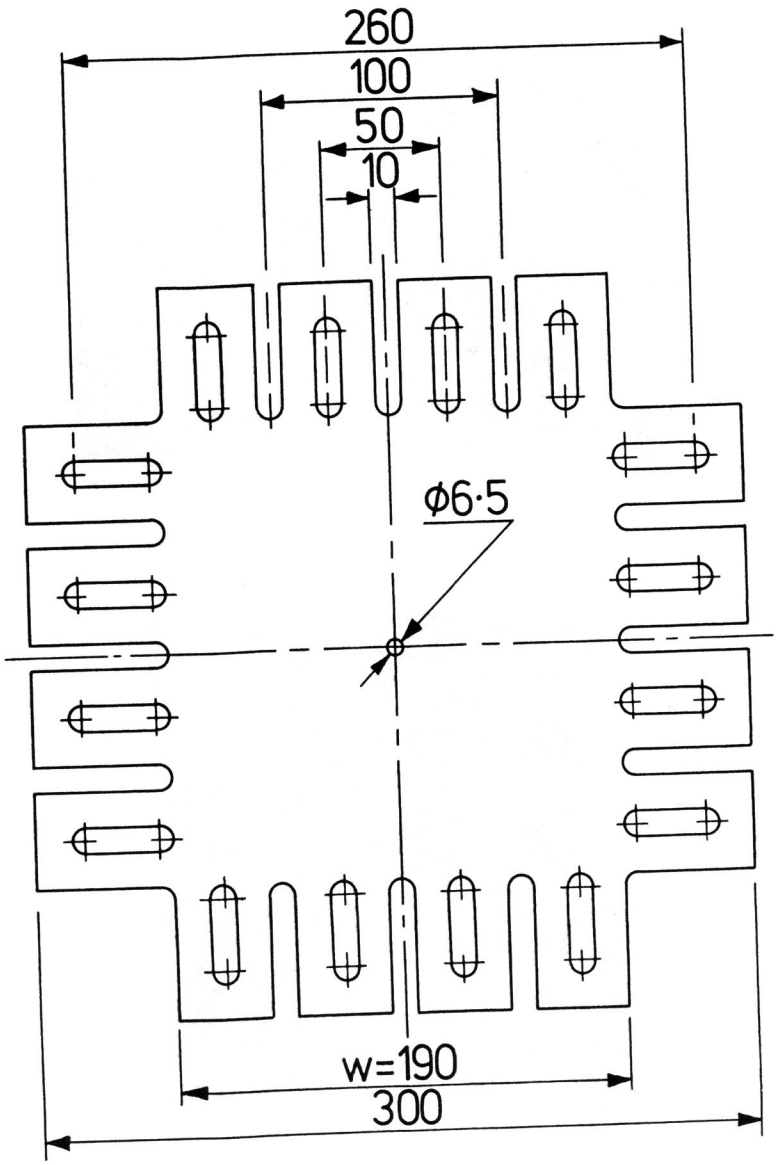

Figure 2: Biaxial fracture specimen design (all dimensions in millimetres).

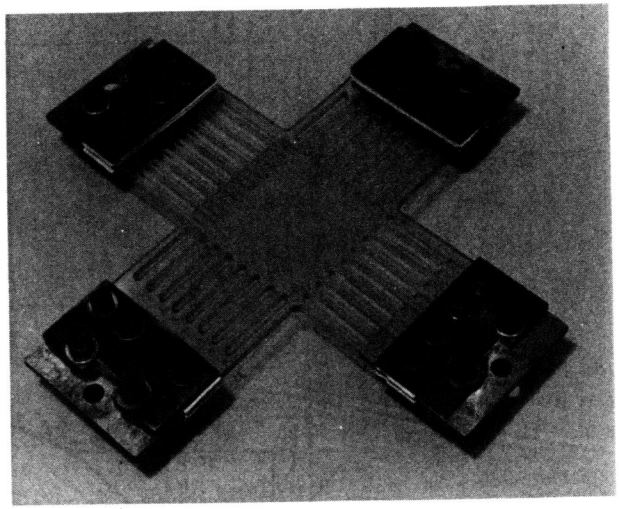

Figure 4: Specimen B with load-distributing shackles.

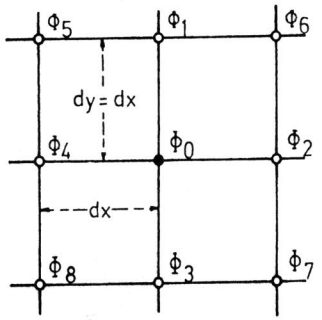

Fig. 5. Net spacings employed for the numerical determination of Laplace's equation.

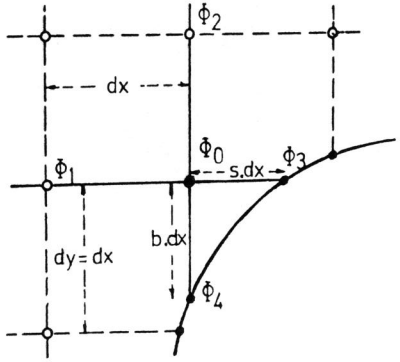

Fig. 6. Net spacings employed near a curved boundary of specimen B.

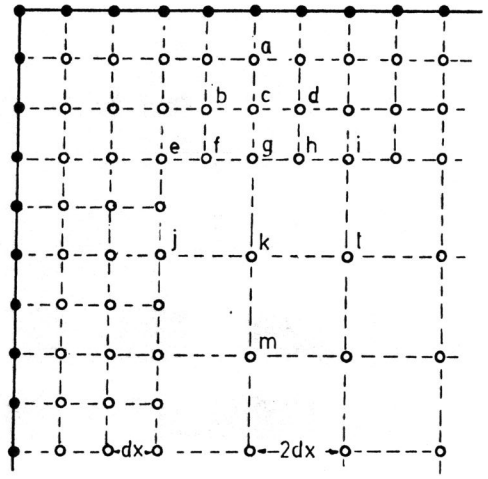

Fig. 7. Change in net spacing.

Table 1. Maximum variance in the values of B_1, σ_y and σ_x.

	Central square of $\frac{3}{4}$ model width			Central square of $\frac{1}{2}$ model width		
Specimen A	B_1	σ_y	σ_x	B_1	σ_y	σ_x
$B_n = 0$	-	9.8 %	-	-	1.1 %	-
$B_n = 2$	7.9 %	7.3 %	11.3 %	.6 %	.5 %	.7 %
Specimen B						
$B_n = 0$	-	6.7 %	-	-	1.1 %	-
$B_n = 2$	4.9 %	2.2 %	5.6 %	.3 %	.3 %	.5 %

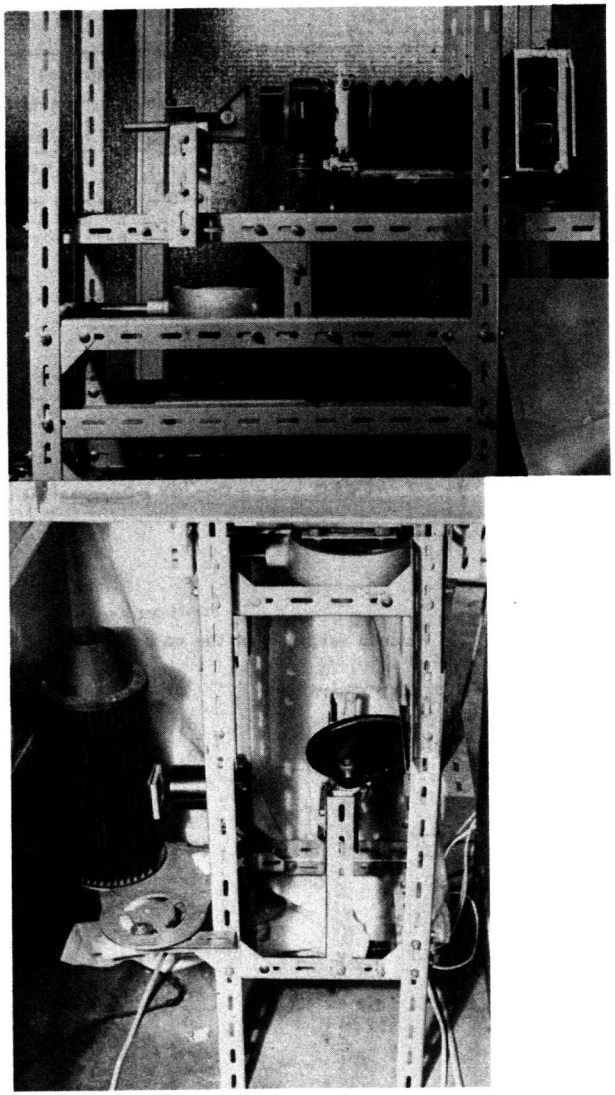

Figures 8 & 9: Arrangement of the lens polariscope.

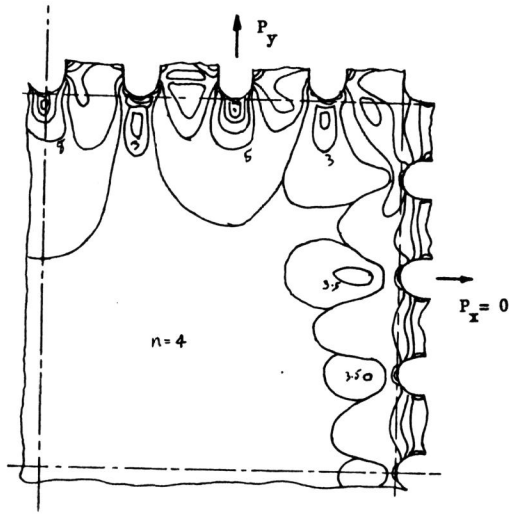

Figure 10: Specimen A - isochromatic pattern for $B_n = 0$.

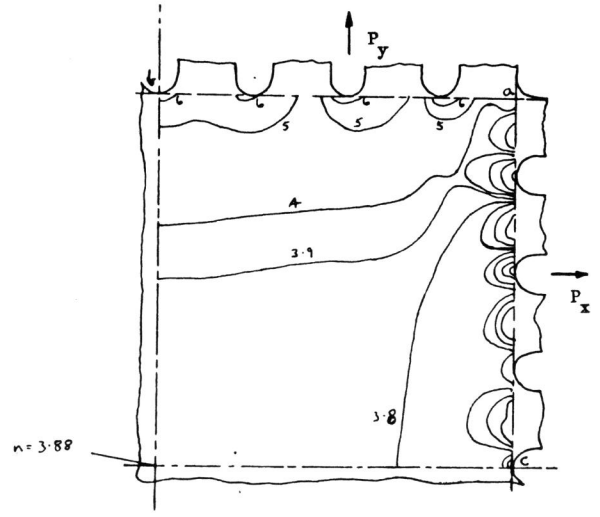

Figure 11: Specimen A - isopachic pattern for $B_n = 0$.

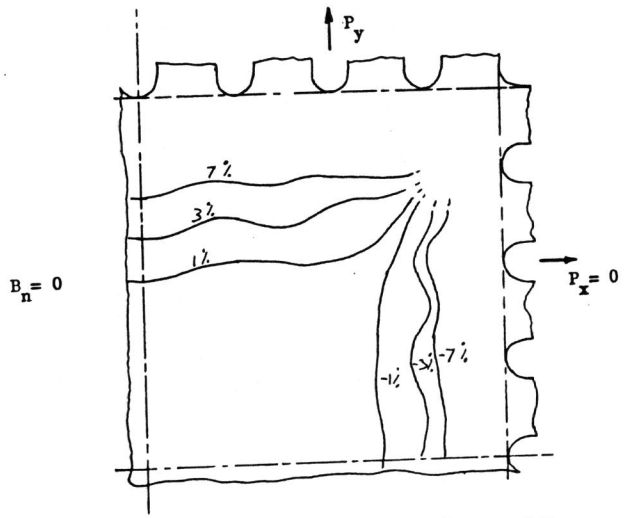

Figure 12: Specimen A - Variation of σ_y as a percentage of σ_y at the centre.

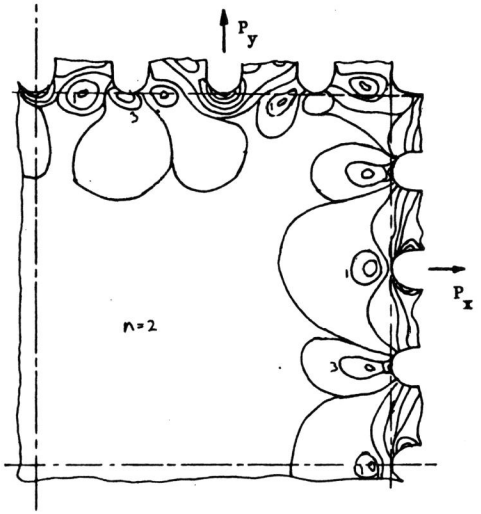

Figure 13: Specimen A - isochromatic pattern for $B_n = 2$.

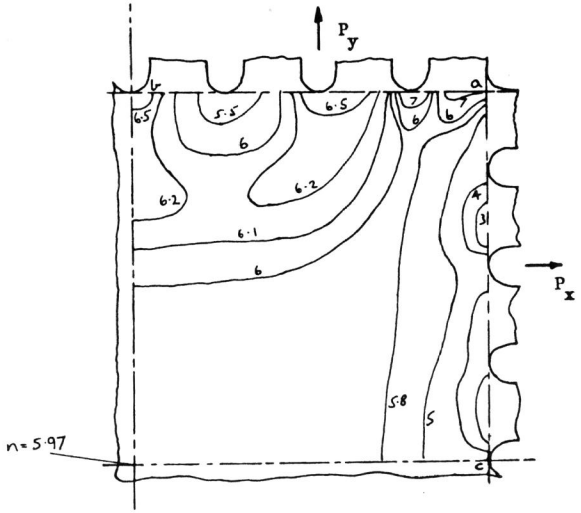

Figure 14: Specimen A - isopachic pattern for $B_n = 2$.

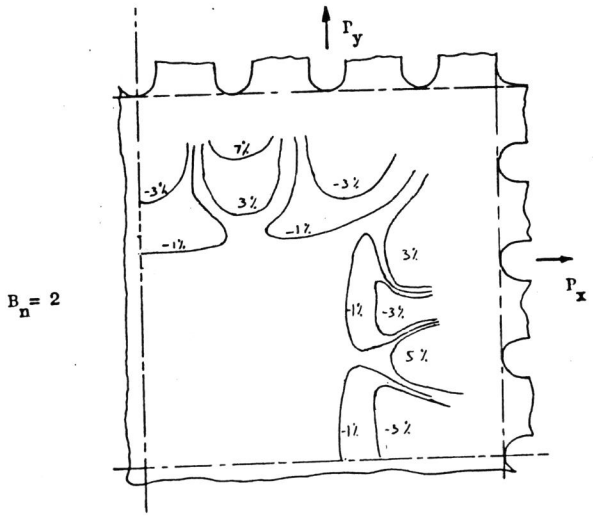

Figure 15: Specimen A - Variation of B_1 as a percentage of B_1 at the centre.

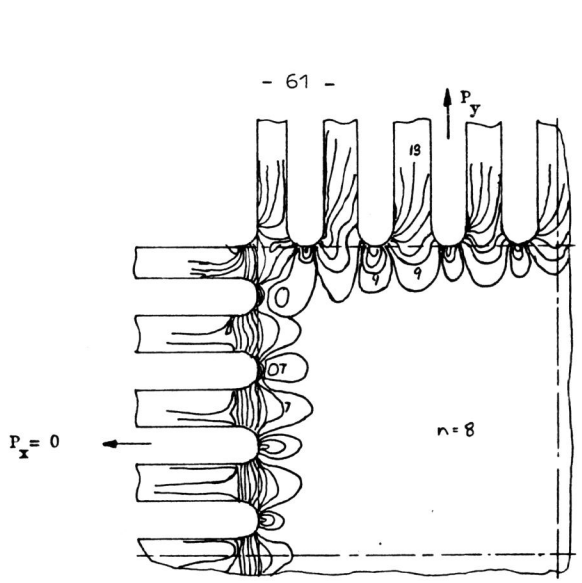

Figure 16: Specimen B - isochromatic pattern for $B_n = 0$.

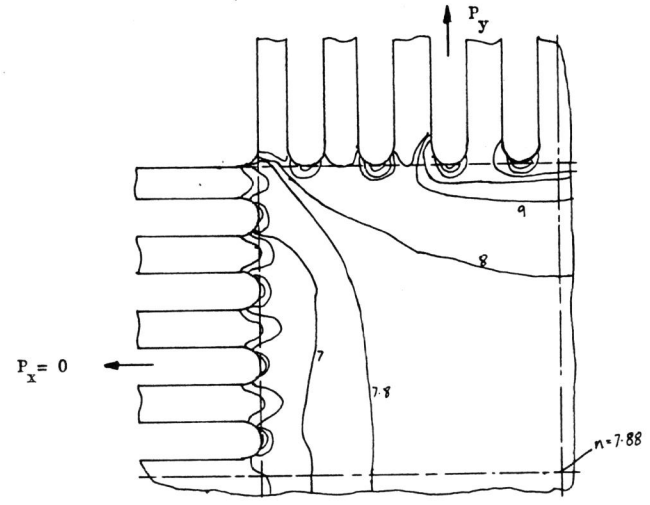

Figure 17: Specimen B - isopachic pattern for $B_n = 0$.

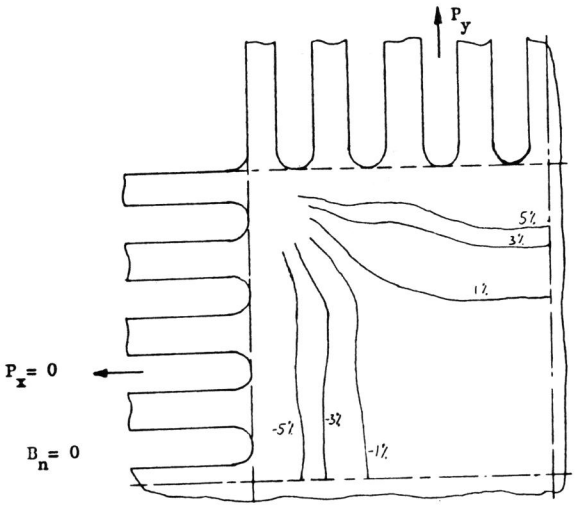

Figure 18: Specimen B - variation of σ_y as a percentage of σ_y at the centre.

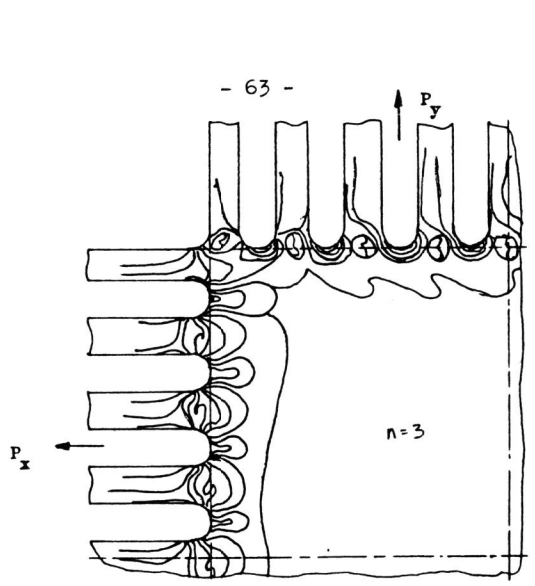

Figure 19: Specimen B - isochromatic pattern for $B_n = 2$.

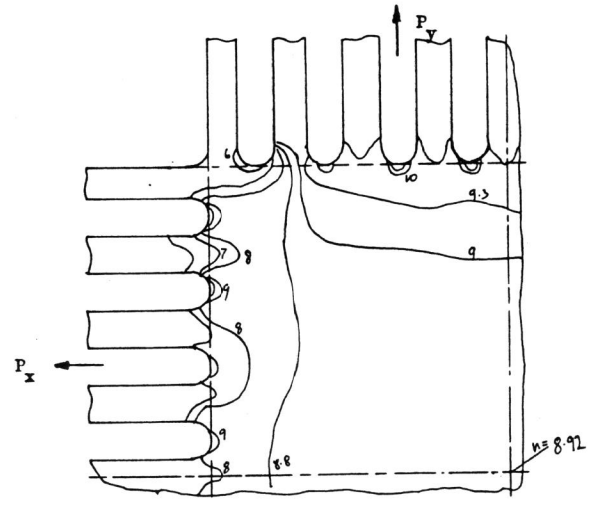

Figure 20: Specimen B - isopachic pattern for $B_n = 2$.

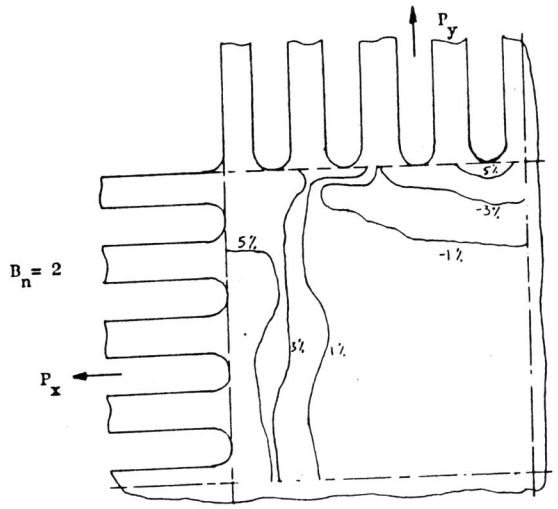

Figure 21: Specimen B - variation of B_1 as a percentage of B_1 at the centre.